Embedding of Precision-Cut Lung Slices in Engineered Hydrogel Biomaterials Supports Extended *Ex Vivo* Culture

Kolene E. Bailey[1], Christopher Pino[2], Mallory L. Lennon[2], Anne Lyons[2], Jeffrey G. Jacot[2], Steven R. Lammers[2], Melanie Königshoff[1], and Chelsea M. Magin[1,2]

[1]Division of Pulmonary Sciences and Critical Care Medicine, Department of Medicine and [2]Department of Bioengineering, University of Colorado, Aurora, Colorado

ORCID IDs: 0000-0002-1272-5055 (J.G.J.); 0000-0002-6988-8584 (C.M.M.).

Abstract

Maintaining the three-dimensional architecture and cellular complexity of lung tissue *ex vivo* can enable elucidation of the cellular and molecular pathways underlying chronic pulmonary diseases. Precision-cut lung slices (PCLS) are one human-lung model with the potential to support critical mechanistic studies and early drug discovery. However, many studies report short culture times of 7–10 days. Here, we systematically evaluated poly(ethylene glycol)-based hydrogel platforms for the encapsulation of PCLS. We demonstrated the ability to support *ex vivo* culture of embedded PCLS for at least 21 days compared with control PCLS floating in media. These customized hydrogels maintained PCLS architecture (no difference), viability (4.7-fold increase, $P < 0.0001$), and cellular phenotype as measured by SFTPC (1.8-fold increase, $P < 0.0001$) and vimentin expression (no change) compared with nonencapsulated controls. Collectively, these results demonstrate that hydrogel biomaterials support the extended culture times required to study chronic pulmonary diseases *ex vivo* using PCLS technology.

Keywords: precision-cut lung slice; hydrogel; biomaterial; three-dimensional printing; pulmonary disease modeling

Chronic respiratory diseases rank among the leading causes of death world wide (1). Although asthma is the most prevalent chronic respiratory disease, chronic obstructive pulmonary disease (COPD) is the fourth leading cause of death by disease in the United States, with a global prevalence of over 250 million patients (2). Current therapeutic options for chronic pulmonary diseases do not halt or reverse disease progression. More effective treatments are needed for patients with chronic conditions, such as asthma, COPD, pulmonary hypertension, interstitial lung disease, and cystic fibrosis. Despite financial investment of over $115 million annually (3), the rate of approval for new respiratory therapies lags behind that of cardiovascular, metabolic, and neurological treatments (1).

Fewer than 10% of respiratory therapies in phase-I testing manifest in a commercially available product (1, 4), due largely to a lack of translation from discovery in an animal model to testing in human clinical trials. Nearly 60% of novel therapeutics fail in phase-II and over 50% of those remaining do not continue beyond phase-III clinical trials (5). Preclinical animal models often exhibit poor

(Received in original form June 28, 2019; accepted in final form September 12, 2019)

Supported by National Institutes of Health (NIH)/National Center for Advancing Translational Sciences Colorado Clinical and Translational Science Award grant UL1 TR002535 and NIH/National Heart Lung and Blood Institute T32 HL007085-43.

Author Contributions: K.E.B. is the primary author responsible for design of experiments in collaboration with C.M.M., and conducted synthesis of hydrogels, preparation of precision-cut lung slices (PCLS), cryostat preparation and slicing, immunostaining, imaging, and preparation of the manuscript. C.P. controlled three-dimensional (3D) printer software and hardware for embedding PCLS, contributed to the Methods section, and reviewed the final manuscript for submission. M.L.L. performed atomic force microscopy (AFM) data collection and analysis, contributed to the Methods section, and reviewed the final manuscript for submission. A.L. assisted with lung architecture evaluation, contributed to the Methods section, and reviewed the final manuscript for submission. J.G.J. supported AFM data collection and analysis and reviewed the final manuscript for submission. S.R.L. constructed 3D printer hardware and wrote 3D printer software, assisted with 3D printing, and reviewed the final manuscript for submission. M.K. provided training and resource support for all PCLS work, and also provided lung biology expertise, experimental design, and reviewed the final manuscript for submission. C.M.M. supervised experimental design, contributed to data collection and analysis, figure generation, and manuscript preparation, and reviewed the final manuscript for submission.

Correspondence and requests for reprints should be addressed to Chelsea M. Magin, Ph.D., University of Colorado, Aurora, CO 80045. E-mail: chelsea.magin@ucdenver.edu.

This article has a data supplement, which is accessible from this issue's table of contents at www.atsjournals.org.

Am J Respir Cell Mol Biol Vol 62, Iss 1, pp 14–22, Jan 2020

Originally Published in Press as DOI: 10.1165/rcmb.2019-0232MA on September 12, 2019
Internet address: www.atsjournals.org

predictivity of human respiratory disease (1, 4). Therefore, a need remains for the development of complementary tools that preserve native human lung structure and function *ex vivo*. These technologies will enable scientists, engineers, and clinicians to study the cellular and molecular pathways underlying respiratory disease progression to advance more precise and efficient therapeutic drug development.

Human-origin *ex vivo* and explant cultures, such as precision-cut lung slices (PCLS), are used with increasing frequency for modeling respiratory pathology (4). PCLS are thin slices of lung tissue that maintain the complex microarchitecture, cellular diversity, and functional response to stimuli observed in native lung tissue, enabling *ex vivo* mechanistic studies of pathogenesis (6). Initial PLCS studies focused on airway constriction that is characteristic of asthma (7), and this technology has since been validated in studies of idiopathic pulmonary fibrosis (IPF) (8, 9), pulmonary hypertension (10, 11), and COPD (12, 13). However, PCLS remain limited by their short duration of viability and functionality *ex vivo*, often reported to be only 7–10 days (13, 14). Over this short duration, PCLS exhibit changes in tissue architecture (14), decreased production of SFTPC (13), and increased proliferation of vimentin-producing mesenchymal cells.

Given the potential clinical impact of PCLS for mechanistic studies and high-throughput drug screening experiments, our goal was to extend the duration of viability and functionality of PCLS in *ex vivo* culture. One study has reported that encapsulation of precision-cut liver slices in Matrigel maintained slice architecture, improved viability, and increased liver-specific metabolism compared with controls over a period of 72 hours (15). Based on the success of this study, we hypothesized that a hydrogel biomaterial could maintain PCLS architecture, viability, and cellular function *in vitro*.

Hydrogels are highly cross-linked polymer networks that absorb large volumes of water while retaining the ability to be created with precise mechanical properties (i.e., stiffness), supplemented with covalently bound cell-adhesive ligands and/or tethered signaling factors, and tuned to degrade on demand. These biomaterials are emerging as ideal extracellular matrix (ECM) mimics for *ex vivo* cell culture applications (16). Integrins expressed in response to specific ligand-binding interactions with the basement membrane or ECM mimics in hydrogel biomaterials are critical for maintenance of cellular homeostasis. Two ligands of particular importance in the pulmonary ECM are fibronectin and laminin, represented by the short peptide sequences, RGDS and YIGSR, respectively, covalently attached to the hydrogel biomaterials presented here to promote integrin binding (17, 18). Specifically, $\alpha_5\beta_1$ (RGDS) and $\alpha_3\beta_1$ (YIGSR) are expressed by cells in the lung (19). RGDS is critical for cellular adhesion to poly(ethylene glycol) (PEG)-based hydrogels (20, 21), and YIGSR is essential for maintaining stemness in epithelial cells (18, 22).

Here, we present a systematic study that varies PEG-based hydrogel thickness as well as RGDS and YIGSR ligand concentration to select the optimal encapsulation procedure for improving PCLS viability and functionality. Quantification and statistical analysis of viability, SFTPC production, vimentin expression, and lung slice architecture allowed us to select an encapsulation method that extends PCLS culture to at least 21 days *ex vivo*. This major technological advance can be easily adopted in any laboratory studying PCLS for early-stage novel target identification and drug discovery. A portion of the work described in this article was published in an abstract in the *Annals of the American Thoracic Society* (23).

Methods

Methods are described in detail in the data supplement.

PCLS Preparation

PCLS were prepared from 6- to 8-week-old C57BL/6J male mice (The Jackson Laboratory) or deidentified human tissue samples (Donor Alliance), as previously described (13). Circular punches 4 mm in diameter were evaluated in all experiments. PCLS samples were cultured in media for at least 18 hours after slicing before encapsulation.

Hydrogel Preparation

Norbornene-functionalized PEG (PEGNB; 8-arm, molecular weight 40 kg/mol), commercially available from JenKem or Creative PEGWorks, was synthesized as previously described (24). PEG-dithiol (molecular weight 3.4 kg/mol) was purchased from Sigma. Peptide sequences that mimic adhesive ligands (CGRGDS and CGYIGSR) were obtained from GL Biochem. The photoinitiator, lithium pheyl-2,4,6-trimethylbenzoylphosphinate, was synthesized as previously described (25), but can be purchased from Sigma. Solutions of 5 weight percent PEGNB, 1 weight percent PEG-dithiol, 0.1–1.0 mM CGRGDS and CGYIGSR (*see* Table E1 in the data supplement), and 1.7 mM lithium pheyl-2,4,6-trimethylbenzoylphosphinate were prepared in HEPES buffering agent (Life Technologies) for mechanical characterization or complete medium for PCLS embedding.

Characterization of Mechanical Properties

The elastic modulus (E) of murine lung tissue samples and hydrogels was measured using parallel-plate rheology (21) and atomic force microscopy (AFM) (26–28), as previously described.

PCLS Embedding and Culture Procedure

PCLS were encapsulated by hand or by three-dimensional (3D) printing (Figure E1). Encapsulation by hand was enabled by constraining hydrogel solutions in a custom-made plastic mold during polymerization. The data presented here were collected from 3D-printed samples for improved accuracy and precision. Embedded PCLS and nonembedded controls were cultured freely floating in 12-well plates in complete media (Dulbecco's modified Eagle medium: Nutrient Mixture F-12 [Gibco]; supplemented with 0.1% FCS [PAA Laboratories]; 100 $U \cdot ml^{-1}$ penicillin, 100 $\mu g \cdot ml^{-1}$ streptomycin, and 2.5 $\mu g \cdot ml^{-1}$ amphotericin B [Sigma]) in a humidified incubator (37°C, 5% CO_2) with media changes every 48 hours (13).

Viability Experiments

A resazurin-based cell viability assay (PrestoBlue; Thermofisher Scientific) was performed at Day 1, 3, 7, 10, 14, 17, and 21, per the manufacturer's instructions.

Immunostaining, Fluorescence Microscopy, and Image Analysis

Embedded and control PCLS were fixed, embedded in optimal cutting temperature (OCT; Thermofisher Scientific) compound, flash frozen, and sectioned (30-μm slices) using a cryostat (Leica CM1850). Immunostaining was completed for SFTPC, E-cadherin, and vimentin with a DAPI counterstain to visualize nuclei. Image analysis was performed using ImageJ software (NIH) to determine the number of SFTPC-positive cells and the area of vimentin coverage. A stereological approach was used to measure lung slice architecture using E-cadherin–stained images (Stereotopix Software; VisioPharm) (29, 30).

Diffusion Experiments

Hydrogels were polymerized at a thickness of 1.1 mm in trans-well inserts (ThinCert; Greiner Bio-One) and partially submerged in PBS. Fluorescently labeled solutions of a small hydrophobic molecule (fluorescein; 376 g/mol) and a large hydrophilic dextran (40 kg/mol) were pipetted on top of the hydrogels and incubated at 37°C. Samples were aliquoted from the PBS at 12, 24, and 48 hours, and fluorescence intensities were measured with a plate reader (Synergy H1 Hybrid Multi-Mode Reader; BioTek).

Statistical Analysis

G*Power statistical software (31) calculated the sample size required ($n = 5$) to ensure over 80% power for detecting an effect size of 1.6 (13) with a Gaussian distribution (one-sided t test, $P < 0.05$). JMP software (SAS Institute) generated nine hydrogel conditions (Table E1) for evaluation. Viability and protein expression results analyzed in the software used a least-squares regression model to determine significance of all factors and plot predicted responses. Parametric or nonparametric one-way and two-way ANOVA tests and tests for multiple comparisons (Tukey and Kruskal-Wallis, respectively) were conducted as appropriate to find significant differences between sample means (95% confidence interval; GraphPad Prism 7 Software; GraphPad Software Inc.). Data are presented as mean (±SEM), normalized to Day 1 results.

Results

Hydrogel Synthesis and Characterization

Encapsulation of precision-cut tissue slices derived from liver within naturally derived hydrogels previously improved viability and functionality over 72 hours in culture (15). Here, we exploited the ability to precisely control both hydrogel elastic modulus (stiffness) and bioactive ligand concentration to design the optimal encapsulation procedure (Figure 1A) for maintenance of PCLS *ex vivo*. As ECM mechanics are a powerful regulator of cellular phenotype (32, 33), the mechanical properties of murine and human lung tissue were characterized. Next, hydrogels were synthesized by reacting PEGNB with a PEG-dithiol cross-linker (Figure 1B). The ratio of reactive groups on the PEGNB to those on the cross-linker was varied from 0.5 to 1.0 to create hydrogels with a range of elastic modulus values (Figure 1C), aiming to match healthy murine tissue values for this study and diseased human tissue values for future experiments. Rheological measurements quantified the shear modulus of murine lung tissue and hydrogel samples, which was converted to elastic modulus assuming a Poisson's ratio of 0.4 for lung tissue (34) and 0.5 for hydrogels (35). Murine lung tissue measured an elastic modulus of 1.45 (±0.08) kPa (Figure 1C). Hydrogel elastic modulus scaled with the ratio of PEG-dithiol (thiols) to PEGNB (-enes) as expected. A ratio of 0.9 resulted in an elastic modulus of 1.17 (±0.07) kPa, not statistically different from healthy mouse lung ($P = 0.071$, Tukey test) (Figure 1C). All subsequent experiments used this ratio to recreate healthy mouse lung mechanics.

AFM quantified the median elastic modulus of healthy ($E = 10.84 \pm 0.74$ kPa) and COPD ($E = 4.06 \pm 0.31$ kPa) human lung tissue as well as a hydrogel formulated to match COPD lung mechanics ($E = 4.99 \pm 0.02$ kPa) (Figure 1D). These results demonstrate a high degree of control over hydrogel mechanics for modeling healthy and diseased ECM mechanics for future studies.

PCLS Embedding

Two different methods of hydrogel encapsulation were performed. Briefly, a bottom layer of hydrogel was pipetted into a plastic mold (Figure E1A) or 3D printed onto a glass slide and polymerized. A 4 mm punch of a PCLS was placed on top of this layer, coated with hydrogel of an equal thickness, and polymerized. PCLS and the encapsulating hydrogels were fluorescently labeled, cryosectioned, and imaged. Measurements and linear regression analysis of overall hydrogel thickness from these images showed that manual encapsulation resulted in less uniform hydrogels with higher variability in total thickness than 3D-printed hydrogels (Figures E1B–E1D). As a result, 3D printing created samples for subsequent experiments to ensure high accuracy and precision when evaluating the impact of hydrogel thickness on biological outputs (Figure 2A).

A multifactorial statistical design determined the minimum number of hydrogel combinations needed to analyze the impact of three variables—encapsulation thickness, RGDS concentration, and YIGSR concentration—on PCLS viability, architecture, and cellular diversity (SFTPC and vimentin expression). This method identified a minimum of nine hydrogel conditions (Table E1) fabricated for testing.

Engineered Hydrogels Improved PCLS Viability, Architecture, and Cellular Function over 21 Days in Culture

Encapsulated PCLS representing all nine hydrogel conditions and nonencapsulated PCLS controls ($n = 5$) were monitored for metabolic activity using the resazurin-based PrestoBlue Cell Viability Reagent (ThermoFisher Scientific). Metabolic activity results normalized to initial readings recorded on Day 1 showed that some hydrogel conditions maintained significantly higher cellular metabolic activity over time than PCLS controls (Figure 2B). The best performing hydrogel improved viability by 4.7-fold ($P < 0.0001$). Based on these results, comparisons between the best-performing hydrogel condition and nonencapsulated controls were performed for architecture and cellular function at Day 21. Representative images of staining for E-cadherin (Figure 2C) show PCLS architecture in nonencapsulated controls and the best-performing hydrogel condition at Days 1 and 21. Stereological analysis of volume-weighted mean alveolar volume and average alveolar tissue area per high-powered field revealed no significant

differences between hydrogel-embedded PCLS and controls and no statistical differences over time (two-way ANOVA, $P > 0.05$; Figure 2D).

Quantification of metabolic activity (Figure 3A), number of SFTPC-positive cells (Figure 3B), and area coverage of vimentin (Figure 3C) on Day 21 was normalized to Day 1 values, revealing one hydrogel condition that improved all three outputs compared with controls. Cellular phenotype, as measured by SFTPC, showed a 1.8-fold increase ($P < 0.0001$), and vimentin expression showed no change compared with nonencapsulated controls. The trend lines resulting from statistical analysis describe the response of each output to every variable tested (Figure 3D) with a predicted optimal hydrogel formulation (0.1 mM RGDS and 0.2 mM YIGSR with a print thickness of 1.1 mm) for maximizing viability and SFTPC production, while minimizing vimentin coverage. The effect magnitude for all

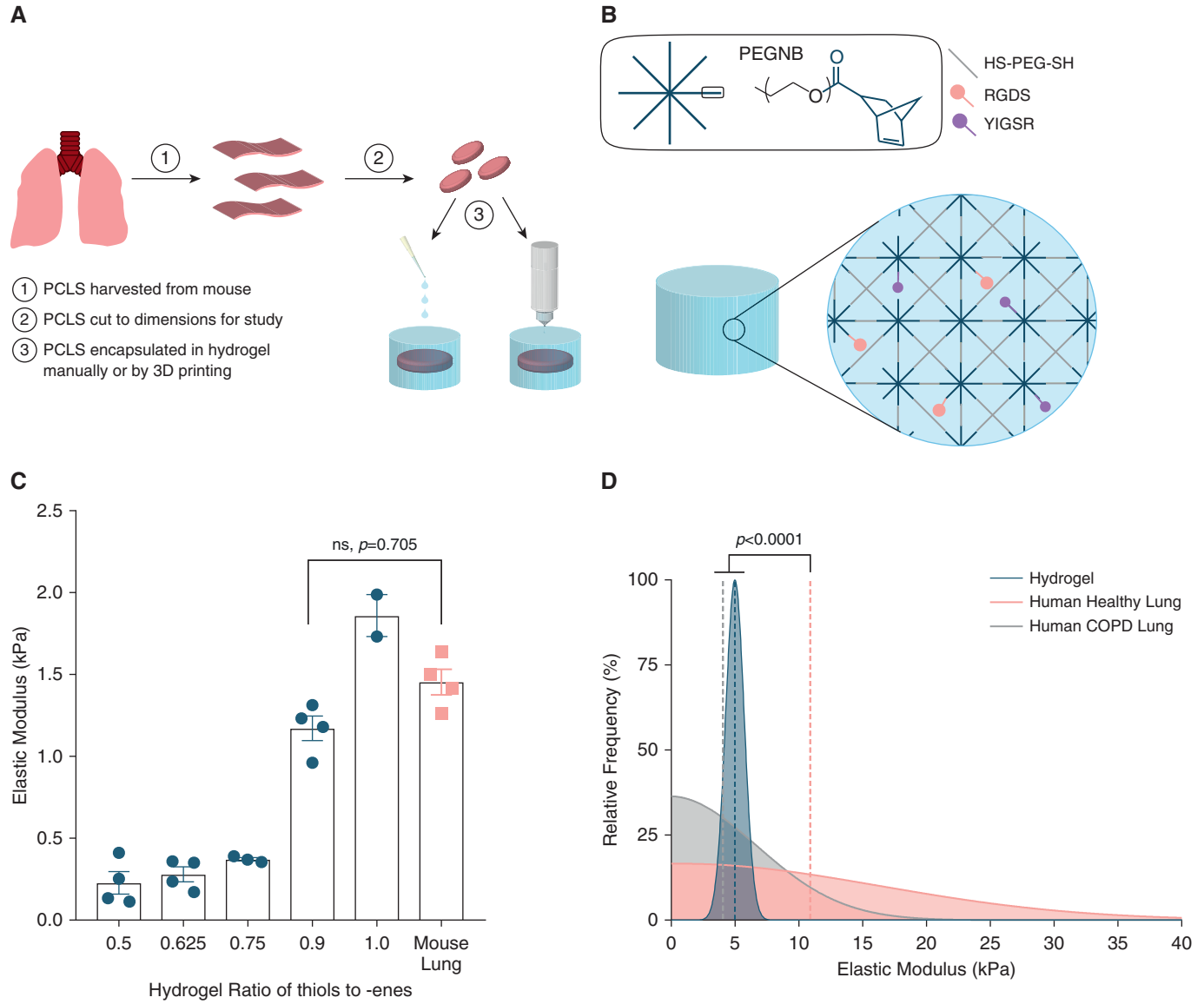

Figure 1. (*A*) Schematic depicting the lung-slicing process. First, precision-cut lung slices (PCLS) were harvested from murine lungs. Slices were cut to 4-mm-diameter punches to ensure uniform tissue quantity for viability and image analysis. Next, PCLS were manually encapsulated, embedded by three-dimensional (3D) printing, or used as controls. (*B*) Hydrogels were synthesized by reacting an eight-arm norbornene-functionalized poly(ethylene glycol) (PEGNB) with a dithiol-functionalized PEG cross-linker and different concentrations of the peptide sequences RGDS and YIGSR via a photoinitiated reaction, forming a step-growth network. (*C*) Bulk rheology of swollen hydrogel bioink samples ($n = 4$) demonstrate that these materials can be designed by varying the ratio of reactive thiol to norbornene groups, creating hydrogels covering a range of physiologically relevant modulus values, including a formulation not statically different from healthy murine lung tissue (parametric one-way ANOVA, Tukey test). Error bars = SEM. (*D*) Atomic force microscopy measurements of human lung samples highlight variation in mechanical properties across tissue samples, as expected ($n = 3$). The median modulus of human chronic obstructive pulmonary disease (COPD) lung tissue was significantly lower than healthy human tissue. A hydrogel formulation designed to match COPD lung tissue mechanics was measured to have a median modulus value not significantly different (ns) from the diseased tissue (nonparametric one-way ANOVA, Kruskal-Wallis test). HS-PEG-SH = PEG-dithiol.

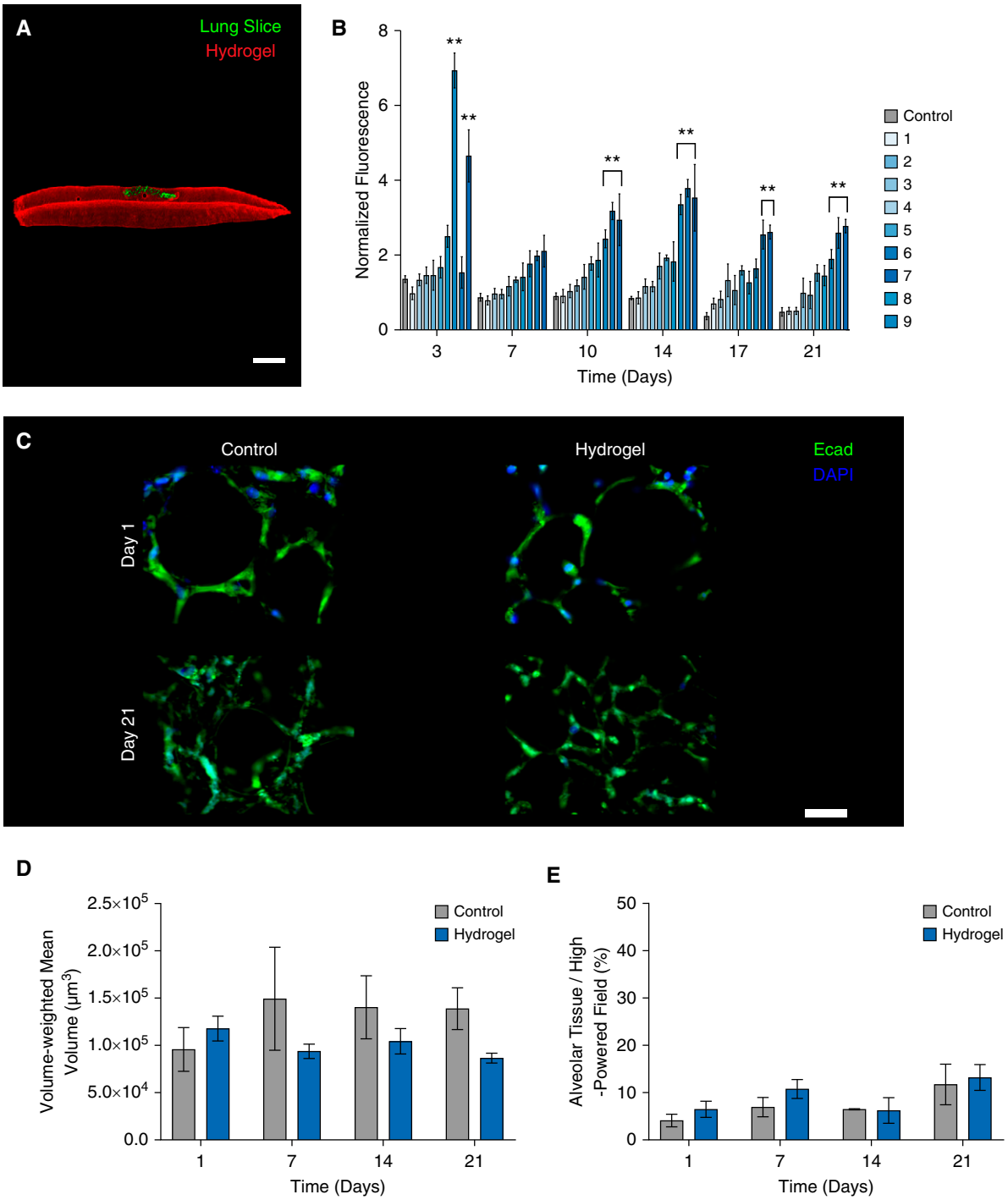

Figure 2. (*A*) Representative images for PCLS (green) embedded within hydrogel (red) show that embedding by 3D printing led to more uniform hydrogel distribution around slices. Scale bar: 1 mm. (*B*) PCLS viability was monitored over 21 days using the PrestoBlue Cell Viability Reagent both in nonembedded PCLS controls and after embedding in nine different hydrogel conditions using 3D printing. Fluorescence intensities normalized to Day 1 show that some hydrogel conditions maintained significantly higher cellular metabolic activity over time than PCLS controls ($n = 5$). $^{**}P < 0.05$ by ANOVA, Tukey test. (*C*) Representative immunofluorescent images in cross-section of nonembedded control and best-performing hydrogel samples stained for DAPI and E-cadherin (Ecad) show that hydrogels support maintenance of PCLS architecture over time. Scale bar: 10 μm. (*D*) Stereological analysis of volume-weighted mean alveolar volume revealed no statistical differences between hydrogel-embedded PCLS and controls, as well as no differences in mean volume over time ($n = 3$). $P > 0.05$, two-way ANOVA. (*E*) Average alveolar tissue coverage per high-powered field measured with stereological techniques shows an increasing trend over time in both sample types, but no significant differences over time, as well as no statistical differences between hydrogel-embedded PCLS and controls ($n = 3$). $P > 0.05$, two-way ANOVA. These results confirm that PCLS architecture is preserved within hydrogel biomaterials over time. Data represent mean ± SEM.

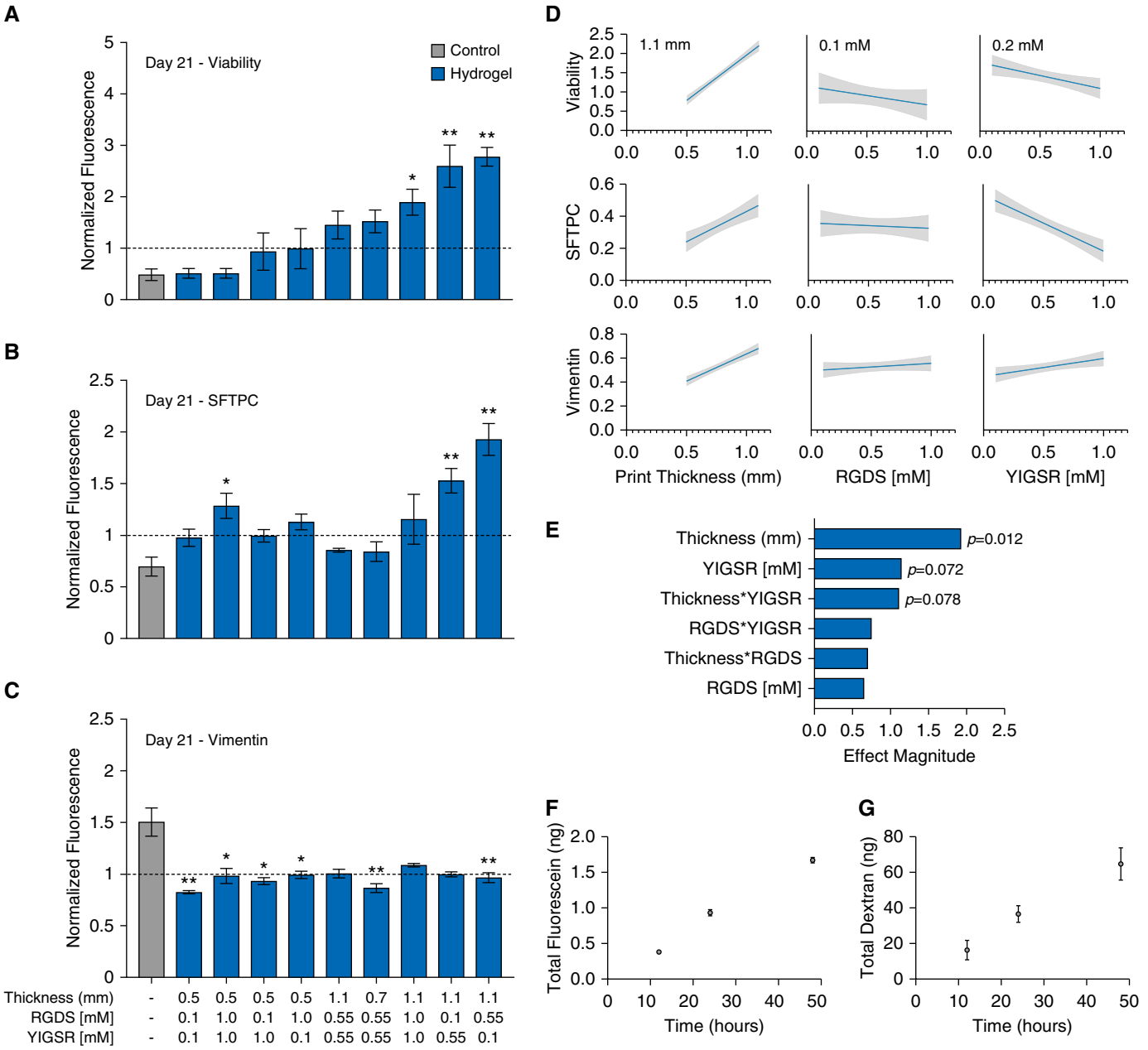

Figure 3. (*A*) Metabolic activity results from Day 21 were normalized to initial readings at Day 1 and indicated that three of the nine hydrogel conditions supported statically higher values of cellular viability compared with nonembedded PCLS controls. All three conditions represented the highest total hydrogel thickness (1.1 mm). (*B*) Quantification of normalized SFTPC data revealed that three hydrogels encouraged increases in the number of SFTPC-positive cells over PCLS controls after 21 days in culture. These results were similarly dependent on total hydrogel thickness. (*C*) Six hydrogel conditions successfully maintained vimentin expression at levels approximately equal to those measured on Day 1. (*D*) Trend lines from the statistical analysis of the design of experiments showed that all three outputs were highly dependent on total encapsulation thickness, not significantly influenced by RGDS concentration, and moderately impacted by YIGSR concentration. These results also gave a predicted optimal hydrogel condition (print thickness = 1.1 mm; RGDS concentration = 0.1 mM; and YIGSR concentration = 0.2 mM) for increasing viability and SFTPC production over time, while minimizing vimentin expression. (*E*) The effect magnitude analysis for all factors and interactions showed that total print thickness, YIGSR concentration, and the interaction between these two factors were the most significant contributors to improved PCLS viability and function within hydrogels. The results from diffusion assays confirmed that both (*F*) fluorescein, a small, hydrophobic molecule, and (*G*) dextran, a large, hydrophilic molecule, were able to diffuse through the full thickness of hydrogel samples. These data indicate that biologically relevant molecules of various sizes and surface energies could be delivered to embedded PCLS to activate specific cellular pathways and/or deliver potential treatments. Error bars = SEM. $n = 5$. $^{*}P < 0.10$ and $^{**}P < 0.05$ by ANOVA, Tukey test.

factors and interactions showed that thickness, YIGSR concentration, and the interaction between these two factors were the most significant contributors to PCLS viability and function within hydrogels (Figure 3E).

Diffusion through Hydrogels Verified Feasible Therapeutic Delivery to Encapsulated PCLS

Two molecules representing a biologically relevant size range (376 g/mol to 40 kg/mol) were selected to evaluate diffusion capacity through the optimal hydrogel formulation (Table E2). Effective diffusion of both test molecules through the full thickness of each hydrogel was measured over 48 hours (Figures 3F and 3G).

Discussion

Translation of novel respiratory therapies from discovery to effective patient treatments remains a challenge. PCLS represent a promising way to bridge this gap, enabling researchers to investigate connections between cellular and organ-level responses in human tissues *ex vivo*. These models are now widely used to address challenges in respiratory toxicology, metabolism, physiology, infection, and pathology (36). Previous studies have shown that PCLS can recapitulate certain aspects of COPD (37) and IPF (9, 38) pathophysiology. Van Dijk and colleagues (37) showed that elastase-treated PCLS exhibited elastin and collagen fiber disorganization, leading to diminished alveolar repair and altered airway mechanics. The optimal timeframe for evaluating airway contractility in these experiments was reported to be between 16 and 52 hours after slicing, and thus limited the collection of further post-treatment time points. Alsafadi and colleagues (9) showed that a mixture of profibrotic growth factors, proinflammatory cytokines, and signaling molecules induced early fibrosis-like characteristics in human PCLS. However, a longer-duration study would be required to observe extensive and irreversible ECM remodeling, a hallmark of IPF *in vivo* (9). The ability to maintain PCLS culture duration for extended periods of time is critical for studying chronic pulmonary diseases. Here, we have established a method for encapsulating PCLS in precisely designed hydrogel biomaterials to extend cellular viability and function for 21 days in culture.

The results in this article highlight the importance of systematically designing the materials used as ECM mimics in 3D cell culture applications. Previous work by van Midwoud and colleagues (15) showed that encapsulation of precision-cut liver slices improved slice viability and liver-specific metabolism in culture; however, the data were limited to 72 hours, because the encapsulation method was not optimized. Liver slices were encapsulated in Matrigel, a commercially available gelatinous protein mixture derived from mouse sarcoma tumor tissue (15). Although Matrigel exhibits inherent bioactivity, this material suffers from batch-to-batch variability of composition and mechanical properties, rendering it challenging to optimize (39). The present study demonstrated that, in addition to matching the mechanical properties of the encapsulating hydrogel to the lung tissue being studied (Figure 1), it was critical to control the thickness of the embedding material as well as the concentration of cell-adhesive ligands. The synthetic PEG-based hydrogels presented here were a highly reproducible platform that supported iterative changes in hydrogel composition and thickness to facilitate optimization. This comprehensive study of several variables revealed that, even though many hydrogels supported PCLS architecture and viability, only one out of the nine hydrogel conditions tested maintained PCLS architecture, viability, and cellular diversity over 21 days in culture (Figures 2 and 3).

Fully synthetic PEG-hydrogels are biologically inert, and can be engineered to present a specific, cell-instructive microenvironment. This feature was leveraged to preserve epithelial–mesenchymal interfaces within embedded PCLS. Prior research has shown that supporting adequate numbers of functional alveolar epithelial type II (ATII) cells within PCLS is important for evaluating the results of studies focused on adult lung remodeling and fibrosis. In fact, two recent reports supported the reparative role of ATII cells to sustain neighboring fibroblasts in a quiescent state with low levels of contractility, proliferation, and matrix production (40). The hydrogel mimics of ECM designed here were fabricated to direct integrin binding and subsequent cellular function without degrading over time (41). Specifically, our group (18) and others have demonstrated that β_1 integrin expression is positively correlated with maintenance of stemness in epidermal epithelial cells (22). For this reason, two short peptide sequences that bind β_1-class integrins expressed by cells in the lung, RGDS ($\alpha_5\beta_1$) and YIGSR ($\alpha_3\beta_1$) (19), were covalently incorporated into encapsulating materials. Statistical analysis revealed that intermediate concentrations of these ligands (0.1 mM RGDS and 0.2 mM YIGSR) supported production of SFTPC by ATII cells (i.e., maintained functionality of ATII cells within PCLS) (Figure 3; $P = 0.072$). Preserving β_1 integrin binding and signaling is one potential mechanism for this improvement over nonembedded controls. Similarly, excess proliferation of mesenchymal cells was prevented by designing the encapsulating hydrogel to be nonbiodegradable (Figure 3). A similar strategy has been shown to limit proliferation of embedded cells due to the small pore size of the molecular network and inability for cells to remodel the material (42). This high level of tunability promoted stability of cellular phenotype and maintenance of epithelial–mesenchymal communication, which will be foundational for improved *ex vivo* models of chronic pulmonary diseases and longer-duration investigations.

In addition to preserving cellular viability and function, this encapsulation procedure can also support induction and subsequent treatment of pathogenic cellular mechanisms. Diffusion results (Figures 3F and 3G) indicated that a range of molecules representing different sizes and surface energies could be adequately delivered through the embedding hydrogel material. Fluorescein (376 g/mol) was used as a surrogate for small hydrophobic molecules, including lysophosphatidic acid (436 g/mol) (38), nintedanib (540 g/mol) (37), and pirfenidone (185 g/mol) (37). FITC-dextran (40 kg/mol) represented larger, more hydrophilic compounds, such as elastase (29 kg/mol) (36) and transforming growth factor-β1 (44 kg/mol). Growth factor and enzyme delivery to PCLS have been studied for induction of chronic disease characteristics to study the molecular mechanisms underlying IPF (9) and COPD (37). Supported by the

embedding process described here, these models can provide the foundation for high-throughput identification of potential molecular targets for drug discovery.

Longer-duration culture of PCLS, especially using human-derived tissue, has broad applications in pulmonary sciences and medicine. In addition to the applications in modeling chronic pulmonary diseases described here, these models can evaluate responses to injury, such as acute hypoxia (43, 44), acute respiratory distress syndrome (45), and COPD or asthma exacerbations, allowing the time needed to both induce injury and monitor the repair and regeneration processes that follow. The PCLS-embedding procedure and precisely designed hydrogel biomaterials reported here are a major technological advance that addresses significant limitations cited in prior PCLS literature. Excitingly, the required polymer components and peptide sequences are commercially available, easy to use, and readily adaptable across all research domains. An open-source scientific community developed the 3D printer and software presented in this report, highlighting a team-science approach that promises rapid development, wide access, and easy sharing of technological advances (46, 47). This model also affords the opportunity to incorporate greater complexity in to the ECM encapsulation, including vascular supply (47), cyclical stretch simulating respiration (48), and addition of other important cell types, such as immune cells (49). Further advances will rapidly scale up high-throughput model systems to support the translation of drugs in development beyond current capabilities. ■

Author disclosures are available with the text of this article at www.atsjournals.org.

Acknowledgment: The authors thank several people who were instrumental to this project. They thank Kristina Hatakka for her help caring for and providing mice from the laboratory of Melanie Königshoff, M.D., Ph.D. They are grateful to Tyler D'Ovidio, B.S., and Dinesh Velu for their assistance with polymer synthesis, figure creation, and custom plastic mold design, as well as Patrick Hume, M.D., Ph.D., and Bradford Smith, Ph.D., for their assistance with stereology measurements. They also thank Darcy Wagner, Ph.D., for conversations and guidance as they were preparing the manuscript.

References

1. Barnes PJ, Bonini S, Seeger W, Belvisi MG, Ward B, Holmes A. Barriers to new drug development in respiratory disease. *Eur Respir J* 2015;45:1197–1207.
2. Soriano JB, Abajobir AA, Abate KH, Abera SF, Agrawal A, Ahmed MB, *et al*.; GBD 2015 Chronic Respiratory Disease Collaborators. Global, regional, and national deaths, prevalence, disability-adjusted life years, and years lived with disability for chronic obstructive pulmonary disease and asthma, 1990–2015: a systematic analysis for the Global Burden of Disease Study 2015. *Lancet Respir Med* 2017;5:691–706.
3. Sertkaya A, Birkenbach A, Berlind A, Eyraud J. Examination of clinical trial costs and barriers for drug development. Washington D.C.: U.S. Department of Health and Human Services; 2014.
4. Mercer PF, Abbott-Banner K, Adcock IM, Knowles RG. Translational models of lung disease. *Clin Sci (Lond)* 2015;128:235–256.
5. Arrowsmith J, Miller P. Trial watch: phase II and phase III attrition rates 2011–2012. *Nat Rev Drug Discov* 2013;12:569.
6. Neuhaus V, Schaudien D, Golovina T, Temann UA, Thompson C, Lippmann T, *et al*. Assessment of long-term cultivated human precision-cut lung slices as an ex vivo system for evaluation of chronic cytotoxicity and functionality. *J Occup Med Toxicol* 2017;12:13.
7. Martin C, Uhlig S, Ullrich V. Videomicroscopy of methacholine-induced contraction of individual airways in precision-cut lung slices. *Eur Respir J* 1996;9:2479–2487.
8. Cedilak M, Banjanac M, Belamarić D, Paravić Radičević A, Faraho I, Ilić K, *et al*. Precision-cut lung slices from bleomycin treated animals as a model for testing potential therapies for idiopathic pulmonary fibrosis. *Pulm Pharmacol Ther* 2019;55:75–83.
9. Alsafadi HN, Staab-Weijnitz CA, Lehmann M, Lindner M, Peschel B, Königshoff M, *et al*. An ex vivo model to induce early fibrosis-like changes in human precision-cut lung slices. *Am J Physiol Lung Cell Mol Physiol* 2017;312:L896–L902.
10. Suleiman S, Klassen S, Katz I, Balakirski G, Krabbe J, von Stillfried S, *et al*. Argon reduces the pulmonary vascular tone in rats and humans by GABA-receptor activation. *Sci Rep* 2019;9:1902.
11. Rieg AD, Suleiman S, Anker C, Verjans E, Rossaint R, Uhlig S, *et al*. PDGF-BB regulates the pulmonary vascular tone: impact of prostaglandins, calcium, MAPK- and PI3K/AKT/mTOR signalling and actin polymerisation in pulmonary veins of Guinea pigs. *Respir Res* 2018;19:120.
12. Van Dijk EM, Culha S, Menzen MH, Bidan CM, Gosens R. Elastase-induced parenchymal disruption and airway hyper responsiveness in mouse precision cut lung slices: toward an ex vivo COPD model. *Front Physiol* 2017;7:657.
13. Uhl FE, Vierkotten S, Wagner DE, Burgstaller G, Costa R, Koch I, *et al*. Preclinical validation and imaging of Wnt-induced repair in human 3D lung tissue cultures. *Eur Respir J* 2015;46:1150–1166.
14. Umachandran M, Howarth J, Ioannides C. Metabolic and structural viability of precision-cut rat lung slices in culture. *Xenobiotica* 2004; 34:771–780.
15. van Midwoud PM, Merema MT, Verweij N, Groothuis GMM, Verpoorte E. Hydrogel embedding of precision-cut liver slices in a microfluidic device improves drug metabolic activity. *Biotechnol Bioeng* 2011; 108:1404–1412.
16. Bailey KE, Floren ML, D'Ovidio TJ, Lammers SR, Stenmark KR, Magin CM. Tissue-informed engineering strategies for modeling human pulmonary diseases. *Am J Physiol Lung Cell Mol Physiol* 2019;316: L303–L320.
17. Gonzalez AL, Gobin AS, West JL, McIntire LV, Smith CW. Integrin interactions with immobilized peptides in polyethylene glycol diacrylate hydrogels. *Tissue Eng* 2004;10:1775–1786.
18. Davis-Hall D, Nguyen V, D'Ovidio TJ, Tsai E, Bilousova G, Magin CM. Peptide-functionalized hydrogels modulate integrin expression and stemness in adult human epidermal keratinocytes. *Advanced Biosystems* 2019;3:1900022.
19. Plosa E, Zent R. Chapter 5—integrin regulation of the lung epithelium. In: Sidhaye VK, Koval M, editors. Lung epithelial biology in the pathogenesis of pulmonary disease. Boston: Academic Press; 2017. pp. 77–89.
20. Hern DL, Hubbell JA. Incorporation of adhesion peptides into nonadhesive hydrogels useful for tissue resurfacing. *J Biomed Mater Res* 1998;39:266–276.
21. Kirschner CM, Alge DL, Gould ST, Anseth KS. Clickable, photodegradable hydrogels to dynamically modulate valvular interstitial cell phenotype. *Adv Healthc Mater* 2014;3:649–657.
22. Watt FM. Role of integrins in regulating epidermal adhesion, growth and differentiation. *EMBO J* 2002;21:3919–3926.
23. Bailey KE, D'Ovidio T, Manning N, Koenigshoff M, Magin CM. Hybrid three-dimensional lung tissue cultures to improve ex vivo models of chronic obstructive pulmonary disease [abstract]. *AnnalsATS* 2018;15: S288.
24. Fairbanks BD, Schwartz MP, Halevi AE, Nuttelman CR, Bowman CN, Anseth KS. A versatile synthetic extracellular matrix mimic via thiol-norbornene photopolymerization. *Adv Mater* 2009;21:5005–5010.
25. Fairbanks BD, Schwartz MP, Bowman CN, Anseth KS. Photoinitiated polymerization of PEG-diacrylate with lithium phenyl-2,4,6-trimethylbenzoylphosphinate: polymerization rate and cytocompatibility. *Biomaterials* 2009;30:6702–6707.

26. Rico F, Roca-Cusachs P, Gavara N, Farré R, Rotger M, Navajas D. Probing mechanical properties of living cells by atomic force microscopy with blunted pyramidal cantilever tips. *Phys Rev E Stat Nonlin Soft Matter Phys* 2005;72:021914.
27. MacKay JL, Kumar S. Measuring the elastic properties of living cells with atomic force microscopy indentation. In: Taatjes DJ, Roth J, editors. Cell imaging techniques: methods and protocols. Totowa, NJ: Humana Press; 2013. pp. 313–329.
28. Liu F, Tschumperlin DJ. Micro-mechanical characterization of lung tissue using atomic force microscopy. *J Vis Exp* 2011;54: 2911.
29. Ochs M, Mühlfeld C. Quantitative microscopy of the lung: a problem-based approach: part 1. Basic principles of lung stereology. *Am J Physiol Lung Cell Mol Physiol* 2013;305:L15–L22.
30. Gundersen HJ, Jensen EB. Stereological estimation of the volume-weighted mean volume of arbitrary particles observed on random sections. *J Microsc* 1985;138:127–142.
31. Faul F, Erdfelder E, Buchner A, Lang A-G. Statistical power analyses using G*Power 3.1: tests for correlation and regression analyses. *Behav Res Methods* 2009;41:1149–1160.
32. Booth AJ, Hadley R, Cornett AM, Dreffs AA, Matthes SA, Tsui JL, *et al*. Acellular normal and fibrotic human lung matrices as a culture system for in vitro investigation. *Am J Respir Crit Care Med* 2012; 186:866–876.
33. Parker MW, Rossi D, Peterson M, Smith K, Sikström K, White ES, *et al*. Fibrotic extracellular matrix activates a profibrotic positive feedback loop. *J Clin Invest* 2014;124:1622–1635.
34. Butler JP, Nakamura M, Sasaki H, Sasaki T, Takishima T. Poissons' ratio of lung parenchyma and parenchymal interaction with bronchi. *Jpn J Physiol* 1986;36:91–106.
35. Gould ST, Darling NJ, Anseth KS. Small peptide functionalized thiol-ene hydrogels as culture substrates for understanding valvular interstitial cell activation and de novo tissue deposition. *Acta Biomater* 2012;8:3201–3209.
36. Sanderson MJ. Exploring lung physiology in health and disease with lung slices. *Pulm Pharmacol Ther* 2011;24:452–465.
37. Van Dijk EM, Culha S, Menzen MH, Bidan CM, Gosens R. Elastase-induced parenchymal disruption and airway hyper responsiveness in mouse precision cut lung slices: toward an *ex vivo* COPD model. *Front Physiol* 2017;7:657.
38. Lehmann M, Buhl L, Alsafadi HN, Klee S, Hermann S, Mutze K, *et al*. Differential effects of Nintedanib and Pirfenidone on lung alveolar epithelial cell function in ex vivo murine and human lung tissue cultures of pulmonary fibrosis. *Respir Res* 2018;19:175.
39. Caliari SR, Burdick JA. A practical guide to hydrogels for cell culture. *Nat Methods* 2016;13:405–414.
40. Tan Q, Ma XY, Liu W, Meridew JA, Jones DL, Haak AJ, *et al*. Nascent lung organoids reveal epithelium- and BMP-mediated suppression of fibroblast activation. *Am J Respir Cell Mol Biol* [online ahead of print] May 3 2019; DOI: 2018-0390OC.
41. Li S, Nih LR, Bachman H, Fei P, Li Y, Nam E, *et al*. Hydrogels with precisely controlled integrin activation dictate vascular patterning and permeability. *Nat Mater* 2017;16:953–961.
42. Bryant SJ, Anseth KS. Controlling the spatial distribution of ECM components in degradable PEG hydrogels for tissue engineering cartilage. *J Biomed Mater Res A* 2003;64:70–79.
43. Desireddi JR, Farrow KN, Marks JD, Waypa GB, Schumacker PT. Hypoxia increases ROS signaling and cytosolic Ca(2+) in pulmonary artery smooth muscle cells of mouse lungs slices. *Antioxid Redox Signal* 2010;12:595–602.
44. Waypa GB, Marks JD, Guzy RD, Mungai PT, Schriewer JM, Dokic D, *et al*. Superoxide generated at mitochondrial complex III triggers acute responses to hypoxia in the pulmonary circulation. *Am J Respir Crit Care Med* 2013;187:424–432.
45. Hess R, Wujak L, Hesse C, Sewald K, Jonigk D, Warnecke G, *et al*. Coagulation factor XII regulates inflammatory responses in human lungs. *Thromb Haemost* 2017;117:1896–1907.
46. Feinberg AW, Miller JS. Progress in three-dimensional bioprinting. *MRS Bull* 2017;42:557–562.
47. Grigoryan B, Paulsen SJ, Corbett DC, Sazer DW, Fortin CL, Zaita AJ, *et al*. Multivascular networks and functional intravascular topologies within biocompatible hydrogels. *Science* 2019;364:458–464.
48. Adkison JB, Miller GT, Weber DS, Miyahara T, Ballard ST, Frost JR, *et al*. Differential responses of pulmonary endothelial phenotypes to cyclical stretch. *Microvasc Res* 2006;71:175–184.
49. Hirahara K, Aoki A, Morimoto Y, Kiuchi M, Okano M, Nakayama T. The immunopathology of lung fibrosis: amphiregulin-producing pathogenic memory T helper-2 cells control the airway fibrotic responses by inducing eosinophils to secrete osteopontin. *Semin Immunopathol* 2019;41:339–348.